Basic Experiments With a Superconducting Full-Bridge Current-Driven Inverter

Quoc Hung Pham and Mathias Noe

***Abstract*—Superconductors have a highly nonlinear current voltage curve that is already used in various applications, such as, for example, in fault current limiters, flux pumps, and persistent mode magnets. It is already known that the dynamic resistance of superconductors can be switched ON and OFF with external magnetic fields. This article applies this knowledge and demonstrates for the first-time experiments with a full-bridge inverter that uses the dynamic resistance of high-temperature superconductors triggered by external magnetic fields as switching elements. For a basic experimental setup, the influence of magnetic field, frequency, and superconductor properties on the behavior of the inverter was investigated. As a result, the principle of a full-bridge current-driven inverter using the dynamic resistance of superconductors and operating in short-circuit output condition is experimentally demonstrated. It is shown that, with reference to the considered short-circuit operation, commutation times down to 5 ms were achieved and that a further reduction is possible by increasing the superconductor length that is exposed to magnetic fields. Long operation times of up to 120 s have been achieved. An upscaling towards faster switching times and higher voltages are possible by further increasing superconductor length.**

***Index Terms*—Coated conductor, loss, inverter, superconductor.**

I. Introduction

SUPERCONDUCTORS exhibit a highly nonlinear current–voltage curve. While exceeding one of their critical values, magnetic field, temperature, or current, the dc resistivity changes from zero to a much higher value. This nonlinear behavior is, for example, used in current limiters [1], [2], [3], [4] when the short-circuit current exceeds the critical current, in thermal switches for persistent magnets [5] and in flux pumps with magnetic field triggered switches, forming a basic rectifier with two switches [6], [7], [8], [9], [10].

It has already been mentioned several times [5], [9], [11], [12] that superconductors can also be used for power converters and rectifiers. Another previous work that investigate the current commutation between parallel paths is shown in [13]. Now four superconducting switches are arranged and connected according to the electric schematic in Fig. 1. This shows a basic H-bridge circuit, which allow ac/dc power conversions.

The authors are with the Karlsruhe Institute of Technology, 76131 Karlsruhe, Germany (e-mail: quoc.pham@kit.edu; mathias.noe@kit.edu).

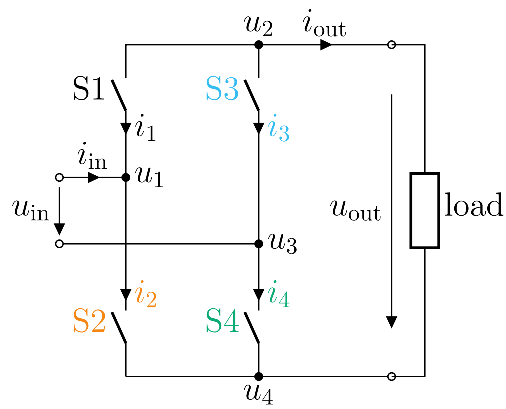

Fig. 1. Schematic of H-bridge circuit.

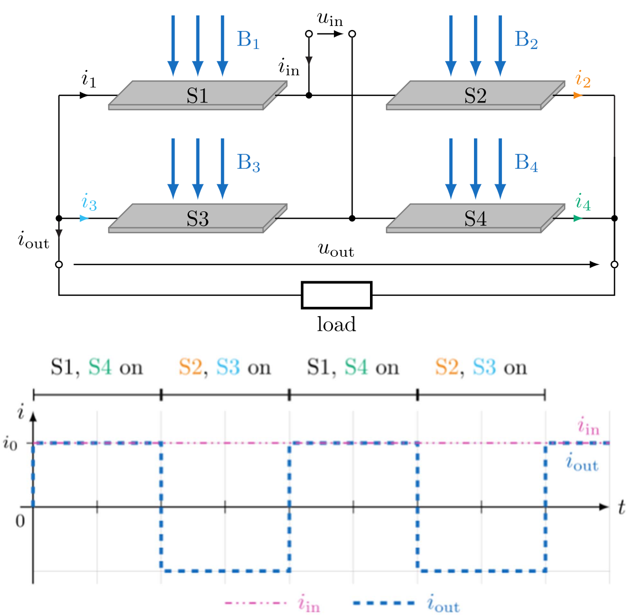

Fig. 2. Schematic of H-bridge based on superconducting dynamic resistance triggered by magnetic fields (top) and input and output current pattern (bottom).

Fig. 2 top shows the general circuit of an H-bridge with four HTS tapes and their connections. It is the main objective of this article that a current pattern shown in Fig. 2 bottom can be achieved, where a dc current at the input is converted in ac currents at the load and the output.

This can be achieved by a controlled triggering of the magnetic fields B1 to B4 in a specific pattern. The on state of a switch is

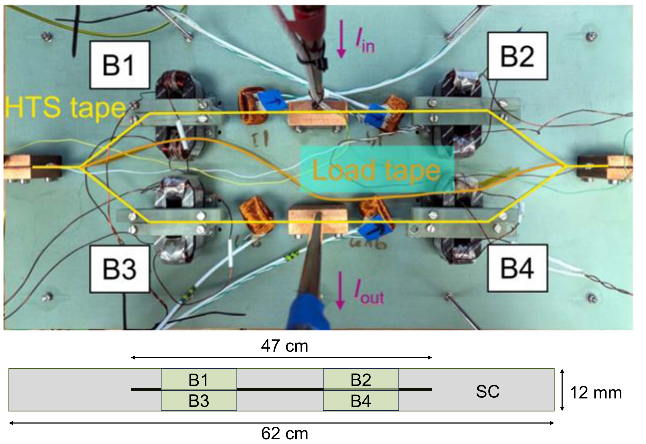

Fig. 3. Photograph of experimental setup (top) and scheme of HTS tape (bottom).

TABLE I
REBCO CONDUCTOR SPECIFICATIONS

Manufacturer	SuperPower
Type	SF12100
Minimal critical current at 77 K, s.f.	380 A
Sample width	12 mm
Thickness of Ag stabilizer layer each side	1.4 µm
Thickness of superconductor layer	1.5 µm
Thickness of substrate	100 µm
Ag resistivity at 77 K	2.7 nΩ m
Substrate resistivity at 77 K	1.23 µΩ m
Resistance per unit length at RT	3.175 mΩ·cm^{-1}
Maximum resistance per unit length* at 77 K	0.729 mΩ·cm^{-1}
Critical temperature	92 K

*Resistance of tape at 77 K with superconducting layer at normal conducting conditions

defined as the state where no external magnetic field is applied to the superconductor, for example, when switch S1 is ON then the magnetic field B1 is OFF. Vice versa, the switch is OFF when the magnetic field is turned ON, and therefore, a dynamic resistance in the superconductor occurs.

There are three stages in the switching pattern. When the switches S1 and S4 are ON and consequently switches S2 and S3 are OFF, then the output current i_{out} is equal to the input current i_{in}.

The output current i_{out} changes then to minus the input current i_{in} when switches S2 and S3 are ON (magnetic fields B2 and B3 are OFF) and switches S1 and S4 are OFF (magnetic fields B1 and B4 are ON). In the default state, all switches are in ON-state (all magnetic fields are OFF), i.e., the input terminals and the input source are short circuited via switches S1 and S4 and S2 and S3. When the input source in the constant current mode is turned ON, the input current is divided between these paths while the output current remains zero.

The objective is to build a fully superconducting current-driven inverter to convert a dc current to an ac current that has a current pattern, as shown in Fig. 2 (bottom). Tests are conducted in short-circuit conditions. The time it takes for the current to commutate between the switches depends on the resistance when the switches are switched OFF. This commutation time is investigated by varying the frequency and magnetic field amplitude of the magnetic field and making additional modifications to the superconductor to increase the resistance. Finally, it is tested whether the circuit is stable and how it behaves during longer running times.

II. EXPERIMENTAL SETUP

The basic experimental setup is shown in Fig. 3, which is then submerged in liquid nitrogen at pool-boiling conditions. A slitted HTS tape with the data from Table I and the dimensions shown in Fig. 3 bottom are used for building the main circuit. Electromagnets B1–B4 are used in each leg of the H-bridge to control the dynamic resistance. The magnetic fields B1–B4 are applied on a tape length of 2 cm. For example, this would result at 1000 Hz and 180 mT in a dynamic resistance of 249.5 $\mu\Omega$ per cm and a built-up resistance of 186.0 $\mu\Omega$ per cm, including the normal conducting layers of the superconductor at 77 K pool boiling. These resistances are measured values from a previous work and details are given in [13] and [14]. The slitted HTS tape marked in yellow is contacted at both ends and in the middle section. The contacts in the middle are the input terminals. An additional 12 mm wide HTS tape is contacted with the outer copper terminals acting as the load of the inverter. This means the output of the circuit is short circuited by a superconducting tape. This setup ensures that there are no contact resistances between the switches S1 and S4. The slitted and the "load" HTS tape are contacted via a face-to-face press contact. The magnets used for the switches are already described in [13] and [14] and have an air gap of 1 mm. Each consists of two U-shaped laminated iron cores with 100 turns of 0.75 mm Cu magnet wire in total. The magnets reach saturation at around 1.4 T.

Each magnet is driven by a separate linear magnet power supply Kepco BOP 72-6, which is controlled by a four-channel arbitrary waveform generator Tabor WW5064 with a trigger delay in the range of 200 ns, leading to a negligible dead time between switching. The bipolar power supply has a minimal slew rate of 0.4 A/μs. To get from 0 A to the maximal output current of 6 A, a time of 15 μs is needed. Triggering the magnets leads to an immediate build-up of dynamic resistance or the delay cannot be measured with a sampling rate of 10 kS/s. The input terminals are connected to a bidirectional dc power supply Keysight RP4943A. The voltages and currents are measured by a nanovolt meter HP 34420A and a digital data acquisition system from National Instruments USB-6281. Self-wound current transducers based on a closed-loop compensated Hall sensor are used to measure the current of each switch. This approach is necessary to separate the electronics from the current pickup coil, which is submerged in liquid nitrogen.

Fig. 4 shows the different tape configurations that were investigated. The total tape resistance is influenced by the thermal behavior of the tape and the Ag layer. Therefore, the bare tape (Config. A) was laminated with a Kapton layer with a thickness of 50 μm on both sides (Config. A Kapton) and the Ag layer was removed at a length of 5 cm in each leg of the HTS tape

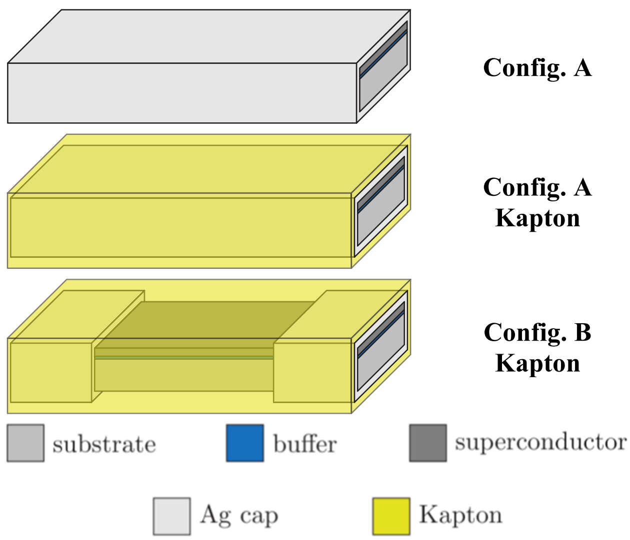

Fig. 4. Scheme of the different tape configurations.

TABLE II
EXEMPLARY RESISTANCE MEASUREMENT RESULTS FOR THE DIFFERENT MEASUREMENTS RESULTS FROM [14]

Configuration	R_{tot} at 500 Hz, 180 mT
Config. A	159 µΩcm^{-1}
Config. A Kapton	225 µΩcm^{-1}
Config. B Kapton	212 µΩcm^{-1}

(Config. B Kapton). The Kapton layer was laminated at a length of 7 cm where the magnetic field was applied. The measured total resistance at 500 Hz and 180 mT for the different configurations is shown in Table II.

III. Basic Switching Experiments

A. Working Principle

With the setup shown in Fig. 3, several basic experiments were performed. The desired current profile is displayed in Fig. 2 (bottom). The magnetic field was varied between zero and 270 mT and the frequency of the magnetic field was set to 500 and 1000 Hz. Fig. 5 shows the current commutation for a magnetic field of 180 mT and a frequency of 1500 Hz for tape configuration A. A constant input dc current of 50 A is applied. When all switches are ON, a slightly unequal current distribution occurs, with 20 A in current paths 2 and 4 and 30 A in current paths 1 and 3. This current is much below the critical current of each path and due to the slitted tape not influenced by the parallel path connections. This current imbalance results therefore in from different contact resistance at the copper in and out current connections.

It can be seen that by switching the magnetic fields B2 and B3 ON (switches S1 and S4 ON), the current in paths 2 and 3 is nearly fully commutated to paths 1 and 4. By changing the magnetic field pattern, the currents change as well and when switching all magnets OFF the current redistributes to the original values. The resulting output current displayed in Fig. 6 show, similar to Fig. 2

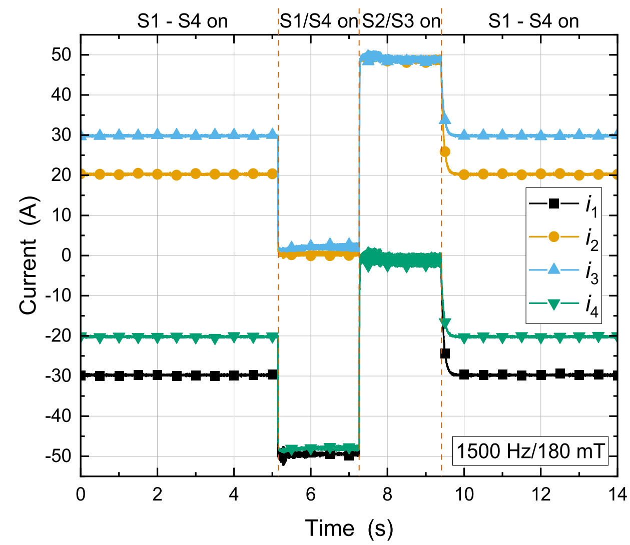

Fig. 5. Current distribution of first switching experiments with superconducting H-bridge circuit (Tape configuration A).

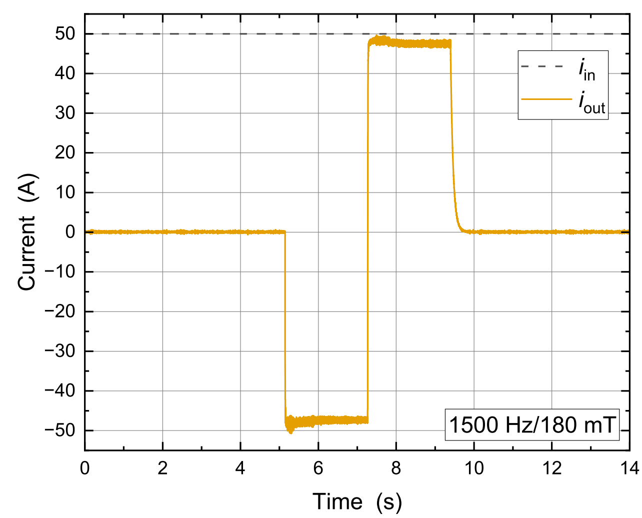

Fig. 6. Input and output currents of the superconducting inverter. Input is a constant current source of 50 A and the resulting output is an alternating rectangular current.

bottom, an alternating rectangular current between -50 and 50 A. In the sections, before 5 s and after 9.5 s, the magnets are turned OFF; therefore, the switches are all turned ON at the same time. This state is intrinsically safe and effectively shorting the input terminals, giving an output current of 0 A. However, it can also be seen that the amplitude is not exactly 50 A. A small part of the input current flows via an OFF-state switch, the so-called leakage current. In this case, the leakage current stabilizes at approx. 2.6 A. The leakage current is highly dependent on the OFF-state resistance of the switches.

In order to achieve high inverter frequencies, the current commutation time needs to be very fast. Fig. 7 shows a detailed view on the current commutation from Fig. 5 and how we determined the commutation time. The commutation time is defined as the time required for the current to change from 10% to 90% of its end value. Both points are marked in the figure with

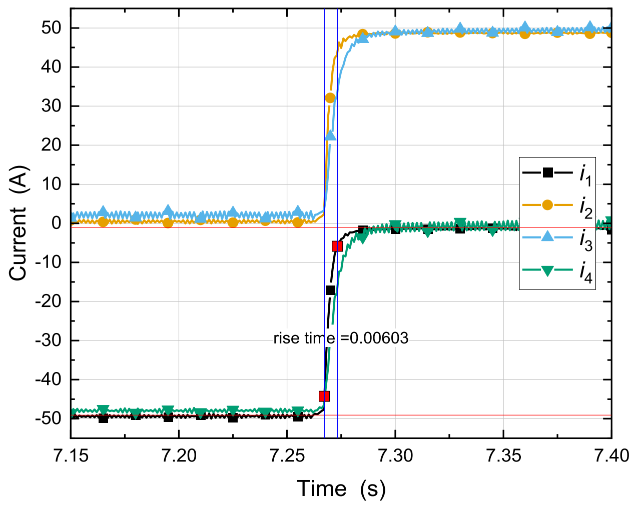

Fig. 7. Current commutation and evaluation of commutation time.

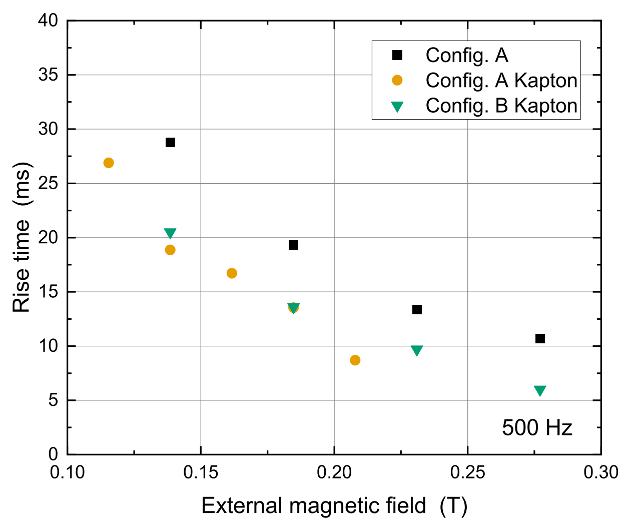

Fig. 8. Comparison of commutation time for different tape configurations at 500 Hz under the variation of magnetic field amplitude.

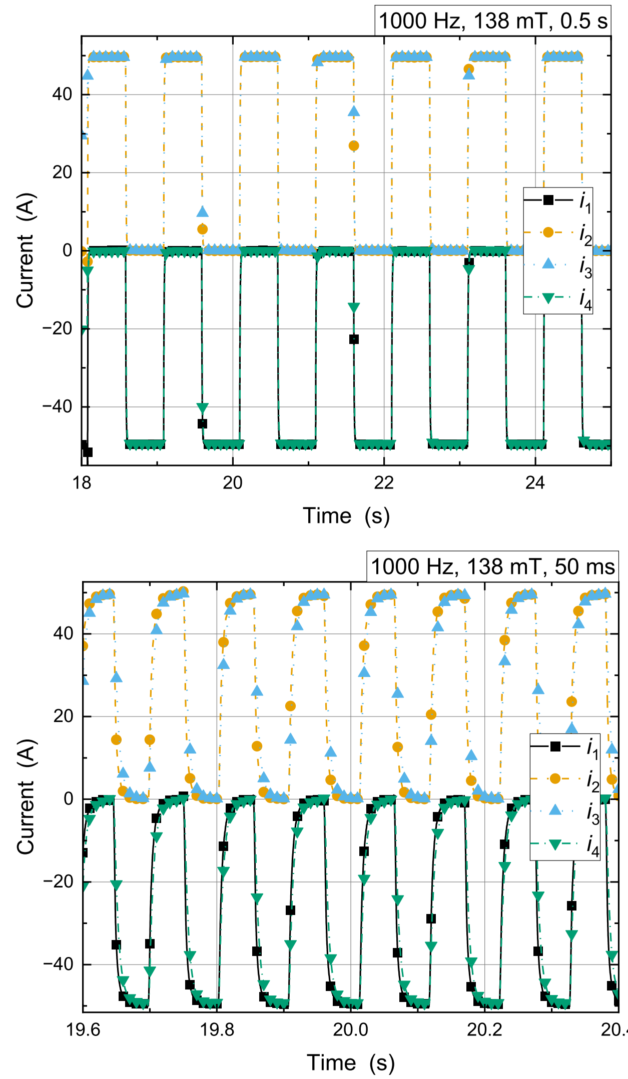

Fig. 9. Current distribution of superconducting H-bridge during continuous stress test. The magnet excitation is 1000 Hz and 138 mT. The switching time is set to 0.5 s (top) and 50 ms (bottom).

a blue vertical line. The time difference between both points is the commutation time.

B. Minimizing Commutation Time

It is clear that the time needed for the current to fully commutate from one current path to another parallel connected path is determined by the resistance R, inductance L, and their ratio R/L. The higher the ratio is, the faster the commutation [13]. Therefore, an increase in dynamic resistance and total resistance of the HTS tape reduces the commutation time. It can be seen in the basic equation of the dynamic resistance given in (1) that this depends on the frequency f, the magnetic field B_{ext}, the transport current I_{t}, the length L, the critical current I_{c0}, and the width of the tape $2w$

$$\frac{R_{sc,\text{dyn}}}{L} = \frac{4\,w}{I_{c0}}\,f\,\left(B_{\text{ext}} - B_{\text{th}}\right) \tag{1}$$

with the threshold magnetic field B_{th} defined as

$$B_{\text{th}} = \frac{4.9284\mu_0 J_{c0} t}{\pi}\,(1-i) \tag{2}$$

and the current density J_{c0}, the tape thickness t, and the ratio between transport current and critical current $i = I_t/I_{c0}$ [15].

In addition, the total resistance is the parallel connection of the dynamic resistance with the resistances of the normal conducting layers. Mainly the silver layer with its lowest resistivity determines the total resistance. The total resistance is calculated by $R_{\text{tot}} = R_{sc} \cdot R_{nc}/(R_{sc} + R_{nc})$ with R_{nc} as the resistance of all nonsuperconducting layers of the HTS tape. In this case, R_{nc} is 0.729 mΩ per cm for configuration A and 11.8 mΩ per cm for configuration B. Measurement results for total resistance can be found in [14].

Fig. 8 shows the commutation time for various magnetic field amplitudes at 500 Hz and different tape configurations. The commutation times are ranging from 28.9 to 6 ms. Configuration

A shows a gradual decrease in commutation time with higher magnetic fields, but overall the highest commutation times. The variants with Kapton have nearly the same values and decreasing with a similar slope compared to the configuration A. Especially at high magnetic fields, a halving of the commutation time can be achieved by adding Kapton insulation to the HTS tape.

These results also agree well with the measured data of the total resistance from [14]. These are remarkably close to each other for Config. A Kapton and Config. B Kapton, as it is also the case here with the commutation time.

IV. Continuous Measurements

For rectifier applications, the superconducting switch is triggered multiple times per seconds for an extended period of time. The HTS tape must withstand such a load without performance loss or thermal runaway. The previous experiments only consisted of a pattern with three pulses; therefore, a continuous stress test is performed. The duration of the test is varied from 20 to 120 s, and the switching periods of the magnet pairs varies from 1 s to 25 ms. The magnetic field amplitude is varied from 46 to 230 mT at 500 and 1000 Hz, respectively.

Fig. 9 shows exemplary the current distribution for 0.5 s (top) and 50 ms (bottom) pulse time. It shows the current of all for switches i_1 to i_4. As expected, one can see the rectangular switching pattern and the current is fully redistributed from one branch to another. Since the switching period and the commutation time are higher in the bottom graph, the current redistribution process is more visible. Both have similar commutation times. The commutation time analysis shows consistent commutation times throughout the whole experiment duration without any change in performance. The commutation time is 10.9 ms for 0.5 s and 11.3 ms for 50 ms. This shows that even with this fast switching, there is sufficient cooldown time between changeovers for the superconductor. A stable operation is possible. In this case the leakage current is only around 0.4 A giving an amplitude of 49.6 A for the rectangular output current.

V. Conclusion

This article shows for the first-time experiments with a full-bridge converter using the dynamic resistance of high-temperature superconductors. Different tape configurations were investigated with different total resistances to investigate their influence on the commutation time of the currents. With the present setup and small length of applied magnetic field of only 2 cm, commutation times of down to 5 ms were achieved. The influence of the magnetic field, the frequency, and the superconductor properties on the basic behavior of the full-bridge converter was investigated. Finally, it was demonstrated that long operation times of up to 120 s have been achieved with reproducible performance. An upscaling toward faster switching times and higher voltages by further increasing superconductor length seems possible.

However, the inverter presented in this work is a demonstrator and a proof of concept and is in no way intended for productive use. Furthermore, the performance at this stage is not in any way comparable with the performance of existing inverters based on semiconductors. Therefore, extensive testing according to current standards was not carried out [16], [17], [18], [19], [20]. The applicable load to the output of the converter is constraint by the built-up resistance of the superconducting switches in OFF-state. In this work, the load is a short circuit with only the contact resistances between superconducting tapes as load. The ratio of load impedance OFF-state resistance determines the current flowing through the switched-OFF switches, the so-called leakage currents, and can be minimized by higher OFF-state resistances. Due to the external alternating magnetic field in the OFF-state of the switch, ac losses are unavoidable. A numerical study about losses has already been conducted in [14], but additional experiments, i.e., electric and/or calorimetric measurement of ac losses or thermal-electric numerical studies, still need to be carried out. Possible applications for a superconducting inverter are low-voltage, high-current applications, where the resistance of the switch in ON-state needs to be low. This is currently realized with many semiconductor modules connected in parallel.

References

[1] M. Noe and M. Steurer, "High-temperature superconductor fault current limiters: Concepts, applications, and development status," *Supercond. Sci. Technol.*, vol. 20, no. 3, Jan. 2007, Art. no. R15, doi: 10.1088/0953-2048/20/3/R01.

[2] S. Elschner et al., "ENSYSTROB – Design, manufacturing and test of a 3-phase resistive fault current limiter based on coated conductors for medium voltage application," *Phys. C Supercond. Appl.*, vol. 482, pp. 98–104, Nov. 2012, doi: 10.1016/j.physc.2012.04.025.

[3] M. Noe et al., "Conceptual design of a 110 kV resistive superconducting fault current limiter using MCP-BSCCO 2212 bulk material," *IEEE Trans. Appl. Supercond.*, vol. 17, no. 2, pp. 1784–1787, Jun. 2007, doi: 10.1109/TASC.2007.898125.

[4] H.-P. Kraemer et al., "ASSiST - A superconducting fault current limiter in a public electric power grid," *IEEE Trans. Power Del.*, vol. 37, no. 1, pp. 612–618, Feb. 2022, doi: 10.1109/TPWRD.2021.3066845.

[5] N. Bykovskiy, A. Dudarev, and H. Kate, "Thermally activated ReBCO switches for charging high-current magnets," *IEEE Trans. Appl. Supercond.*, vol. 29, no. 5, Aug. 2019, Art. no. 5502005, doi: 10.1109/TASC.2019.2895849.

[6] J. Ma et al., "A numerical design of high-resistance and energy-efficient HTS switch based on dynamic resistance," *IEEE Trans. Appl. Supercond.*, vol. 33, no. 5, Aug. 2023, Art. no. 5401605, doi: 10.1109/TASC.2023.3252493.

[7] J. D. D. Gawith et al., "A half-bridge HTS transformer–rectifier flux pump with two AC field-controlled switches," *Supercond. Sci. Technol.*, vol. 31, no. 8, Jan. 2018, Art. no. 085002, doi: 10.1088/1361-6668/aac86d.

[8] B. Leuw, J. Geng, J. H. P. Rice, D. A. Moseley, and R. A. Badcock, "A half-wave superconducting transformer-rectifier flux pump using J_c (B) switches," *Supercond. Sci. Technol.*, vol. 35, no. 3, Mar. 2022, Art. no. 035009, doi: 10.1088/1361-6668/ac4f3d.

[9] L. J. M. Van De Klundert and H. H. J. Ten Kate, "Fully superconducting rectifiers and fluxpumps Part 1: Realized methods for pumping flux," *Cryogenics*, vol. 21, no. 4, pp. 195–206, Apr. 1981, doi: 10.1016/0011-2275(81)90195-8.

[10] H. H. J. ten Kate, P. B. Bunk, R. B. Britton, and L. J. M. van de Klundert, "High current and high power superconducting rectifiers," *Cryogenics*, vol. 21, no. 5, pp. 291–296, May 1981, doi: 10.1016/0011-2275(81)90006-0.

[11] J. D. D. Gawith et al., "An HTS power switch using YBCO thin film controlled by AC magnetic field," *Supercond. Sci. Technol.*, vol. 32, no. 9, Jan. 2019, Art. no. 095007, doi: 10.1088/1361-6668/ab2d61.

[12] J. Geng, R. A. Badcock, and C. W. Bumby, "A wireless rectifier for inductively energizing high direct-current high-temperature superconducting magnets," *IEEE Trans. Ind. Electron.*, vol. 68, no. 4, pp. 3273–3281, Apr. 2021, doi: 10.1109/TIE.2020.2982095.

[13] Q. H. Pham, M. Noe, and A. Kudymow, "Magnetic field triggered switching of high-temperature superconductors—Basic experiments," *IEEE Trans. Appl. Supercond.*, vol. 35, no. 2, Mar. 2025, Art. no. 5000107, doi: 10.1109/TASC.2024.3514180.

[14] Q. H. Pham, R. Nast, and M. Noe, “Resistance of high-temperature superconducting tapes triggered by alternating magnetic field,” *IEEE Trans. Appl. Supercond.*, vol. 35, no. 3, May 2025, Art. no. 1800208, doi: 10.1109/TASC.2025.3550837.

[15] H. Zhang, B. Shen, X. Chen, and Z. Jiang, “Dynamic resistance and dynamic loss in a ReBCO superconductor,” *Supercond. Sci. Technol.*, vol. 35, no. 11, Nov. 2022, Art. no. 113001, doi: 10.1088/1361-6668/ac95d5.

[16] *IEEE Standard for Interconnection and Interoperability of Distributed Energy Resources with Associated Electric Power Systems Interfaces*, IEEE Std 15472-2023 Revis. IEEE Std 15472-2008, 2024, doi: 10.1109/IEEESTD.2024.10534228.

[17] F. Ashrafidehkordi, X. Liu, and G. De Carne, “Impedance-based stability analysis of a power hardware-in-the-loop for grid-following inverter testing,” in *Proc. IEEE Energy Convers. Congr. Expo.*, 2023, pp. 1116–1121, doi: 10.1109/ECCE53617.2023.10362808.

[18] F. Katiraei, K. Atef, K. Salem, T. Chang, B. Koosha, and A. Momeni, “Power hardware-in-loop testing of advanced inverter functionalities,” in *Proc. IEEE 43rd Photovolt. Specialists Conf.*, 2016, pp. 1381–1386, doi: 10.1109/PVSC.2016.7749841.

[19] J. Peralta, D. Calderon, L. Estrada, J. Ortega, N. Vazquez, and C. Limones, “Semi-custom HIL simulation of a three-phase power inverter,” in *Proc. IEEE Int. Conf. Eng. Veracruz*, 2023, pp. 1–6, doi: 10.1109/ICEV59168.2023.10329657.

[20] K. Deepak, Y. Hazarathaiah, M. V. Vardhan, S. Naseer, S. Y. Rao, and T. Rakesh, “Performance evaluation of five and seven level H-bridge inverter under change in modulation index by using hardware - in the - loop,” in *Proc. Int. Conf. Sustain. Commun. Netw. Appl.*, 2023, pp. 813–818, doi: 10.1109/ICSCNA58489.2023.10370656.